Accepted for publication in IEEE Transactions on Nuclear Science, June, 1999.

A New X-ray Computed Tomography System for Laboratory Mouse Imaging[1]

M. J. Paulus, *Member, IEEE,* H. Sari-Sarraf, *Member, IEEE,* S.S. Gleason, *Member, IEEE,*
M.Bobrek, *Member, IEEE,* J. S. Hicks, *Member, IEEE,* D. K. Johnson
J. K. Behel, *Student Member, IEEE,* L. H. Thompson, *Student Member, IEEE,*
and W. C. Allen, *Student Member, IEEE*

Oak Ridge National Laboratory
P.O. Box 2008, Oak Ridge, Tennessee 37831-6006

Abstract

Two versions of a new high-resolution x-ray computed tomography system are being developed to screen mutagenized mice in the Oak Ridge National Laboratory Mammalian Genetics Research Facility. The first prototype employs a single-pixel cadmium zinc telluride detector with a pinhole collimator operating in pulse counting mode. The second version employs a phosphor screen/CCD detector operating in current mode. The major system hardware includes a low-energy x-ray tube, two linear translation stages and a rotational stage. For the single-pixel detector, image resolution is determined by the step size of the detector stage; preliminary images have been acquired at 100 μm and 250 μm resolutions. The resolution of the phosphor screen detector is determined by the modulation transfer function of the phosphor screen; images with resolutions approaching 50 μm have been acquired. The system performance with the two detectors is described and recent images are presented.

I. INTRODUCTION

The Oak Ridge National Laboratory established a small animal genetics program soon after World War II to assess the biological effects of ionizing radiation in mammals. Experiments were carried out to determine both rates of induction of germline mutations and differential sensitivities of germ cell stages to induced damage in mice. In more recent experiments, mutagenesis has also been carried out using a wide variety of chemicals. This program provided the data upon which assessments of human health risk following radiation exposure are based and led to the establishment of the largest experimental mouse colony in the world.

The Oak Ridge colony currently houses more than 70,000 mice representing about 400 mutant lines. Each time a mutagenesis experiment is performed, the mice must be screened for the presence of mutations. Typically more than 500 mice are produced for each observed phenotype. The screening process currently depends largely on physical examination and behavioral analysis of the mice and is both time consuming and costly.

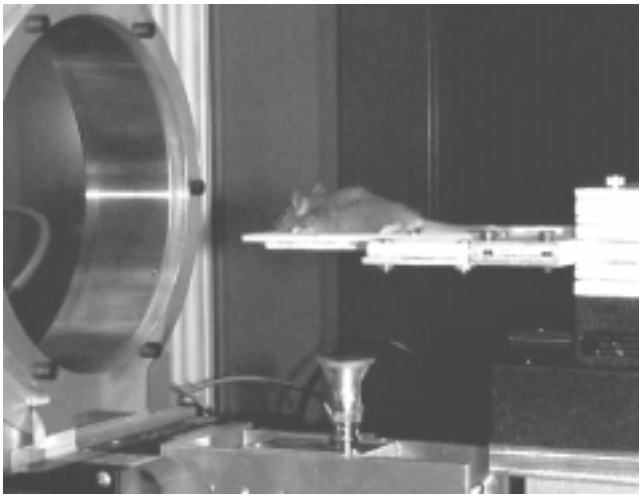

Figure 1. Prototype MicroCAT scanner using a single-pixel CZT detector.

In order to accelerate the screening process and reduce the per-animal screening costs, a new x-ray computed tomography system has been designed specifically for mouse screening. Several other teams have recently reported high-resolution small-animal positron emission tomography (PET) [1,2], single photon emission tomography (SPECT) [3-4], and magnetic resonance imaging (MRI) [5,6] systems. Considerable work has also been reported in the development of x-ray microtomography systems for *ex vivo* specimen studies [7-9], and several laboratories have also designed x-ray computed tomography (x-ray CT) systems for *in vivo* small animal imaging [10-13]. The goals for the small animal imaging system development described here are to minimize the fabrication and operation costs, achieve a high data acquisition rate (nominally a minute per data set), and provide high-resolution anatomic images (nominally 50 μm FWHM). We believe x-ray CT is the optimal modality for meeting these cost, resolution and throughput objectives.

Two micro-computed tomography (MicroCAT) detector configurations are explored. The first is a single-pixel cadmium zinc telluride (CZT) detector with a 100-μm diameter collimator. With this detector the MicroCAT

[1]Research sponsored by the Laboratory Directed Research and Development Program of Oak Ridge National Laboratory, managed by Lockheed Martin Energy Research Corp. for the U.S. Department of Energy under Contract No. DE-AC05-96OR22464.

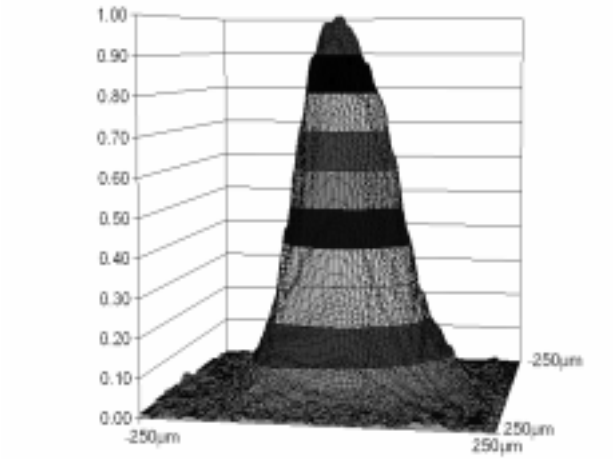

Figure 2. Measured point spread function of the MicroCAT x-ray tube. The profile is well described by a 2-D gaussian function with σ_x = 71.5 μm and σ_y = 50.5 μm.

operates as a first/second generation scanner in which the collimated detector is translated across the field of view for each projection. The second configuration employs a high-resolution CCD/phosphor screen area detector. With this device the MicroCAT functions as a third generation scanner, acquiring up to 1024 parallel slices in a single acquisition.

II. SYSTEM DESCRIPTION

A. Hardware

Shown in Figure 1 with the single-pixel CZT detector, the MicroCAT scanner consists of two linear translation stages (patient bed and detector) with < 25-μm positional accuracy and a rotational stage with < 0.002-degree positional accuracy. The x-ray source is a commercially available 50W tungsten anode tube with a thin beryllium window, maximum voltage of 50 kV_p and maximum anode current of 1 mA [14]. The focal spot is well modeled as a 2-D gaussian function with σ_x = 71.5 μm and σ_y = 50.5 μm (Figure 2).

The scanner is mounted on an optical table for vibration isolation and housed in a tin-doped Plexiglas radiation enclosure. Scanner motion and data acquisition are controlled by a Windows NT workstation.

Single-Pixel CZT Detector

The single-pixel CZT detector is a commercially available 3 mm^3 device [15] with a thin beryllium window and a custom 100-μm diameter copper collimator. CZT detects x-rays through direct absorption in the semiconductor bulk producing approximately one electron-hole pair per 5 eV of absorbed photon energy. Ultimately the maximum pulse-rate is limited by the effective hole mobility (4.7 $cm^2V^{-1}s^{-1}$) [16] which is significantly lower than the effective electron mobility (690 $cm^2V^{-1}s^{-1}$) [16]. For this application the detector is biased at +100V where the

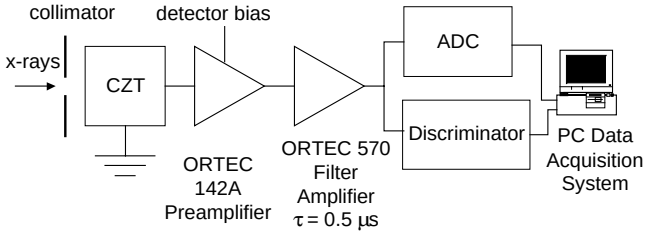

Figure 3. Schematic diagram of the collimated single pixel CZT detector and readout circuitry.

positive terminal is located on the backside of the detector opposite the entrance window. The low energy photons emitted by the x-ray source are absorbed primarily through photoelectric interactions near the surface so that the holes travel a much shorter distance than the electrons. The read-out electronics (Figure 3) include a commercial charge-sensitive preamplifier [17] and semi-gaussian filter amplifier [18]. We estimate the detector collection time to be on the order of a few hundred nanoseconds [16], ensuring nearly complete charge collection with the 0.5 μs shaping time selected for the filter amplifier. The filter amplifier drives a custom leading-edge discriminator and a custom flash analog-to-digital converter, which in turn drive a data acquisition (DAQ) card in the personal computer.

Figure 4 shows measured x-ray spectra obtained with the collimated CZT detector as a function of the x-ray source high voltage. The spectra were obtained using a 1024 channel MCA [19] coupled to the output of the filter amplifier in Figure 3. The MCA scale was calibrated using Cd-109 and Am-241 test sources. The detector noise floor is approximately 7 keV and the peaks associated with the L-shells of the x-ray source tungsten target are clearly evident.

Although a collimator is used with the single-pixel CZT detector described here, no collimation is planned for the CZT area detector under development or the CCD/phosphor screen detector described below. With the low energy x-rays used here photoelectric absorption is the dominant attenuation mechanism. (For 20 keV x-rays the photoelectric attenuation coefficient is ~2.6 times greater than that of Compton scatter for soft tissue and ~20 times

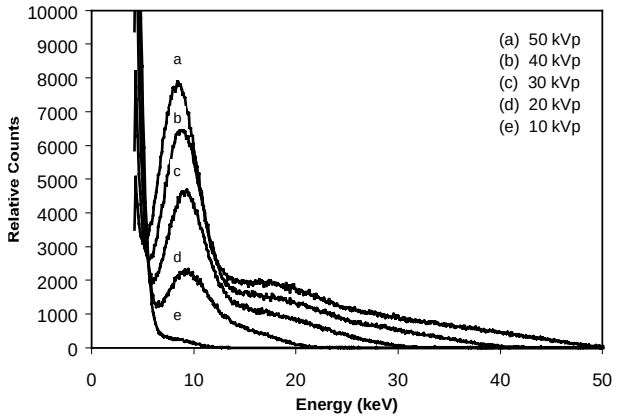

Figure 4. Measured x-ray spectra obtained using the collimated single pixel CZT detector.

greater than that of Compton scatter for bone). Without collimation, scatter will degrade the soft tissue contrast somewhat, but the increased x-ray flux and simplification of the detector design are believed to justify the compromise.

For tomographic data acquisitions the collimated detector is translated across the projection in 250-μm steps, setting the limit on the reconstructed image resolution. (The fan-beam architecture of the scanner reduces the sampling step size to to ~175 μm in the center of the field of view). In order to acquire an image slice in a reasonable period of time, the detector remains in each position for 0.1 sec. Thus, for 2-inch wide projections, each projection is acquired in ~20 seconds and a typical data set of 360 projections requires a total scan time of ~2 hours per slice.

The pulse counting architecture has two advantages in x-ray CT. First, because each x-ray is individually observed, it is possible to incorporate the energy dependence of the x-ray attenuation into the data set. Traditional "current-mode" CT systems measure average attenuation coefficients for the x-ray tube spectrum; knowledge of the energy dependent x-ray attenuation should provide greater contrast between tissue types [20,21]. The energy data may also be used to correct for beam hardening. Second, the collimated pulse-mode detector may be used to SPECT data as well as CT data; if the x-ray energies are well below the SPECT γ-ray energies it is even possible to acquire data for both modalities simultaneously. Emission-Transmission Computed Tomography (ETCT) can provide correlated anatomical and physiological images as well as excellent quantification of *in vivo* radionuclide activity [22].

The principal disadvantage of the pulse counting detector compared with a current-mode detector is the lower x-ray throughput. Because of the per-pulse dead time of the pulse-counting system, it is impossible to acquire data sets with statistics comparable to those of current mode systems. We are working to assess the trade-off between the availability of energy information and reduced statistics. A 2-sided CZT strip detector has been designed and fabricated for this project and will be tested when the integrated read-out circuitry is completed.

Phosphor Screen/CCD Detector

A CCD/phosphor screen detector [23] has also been used to acquire images. The detector employs a Kodak KAF-1000 CCD array with an active area of 24.6 X 24.6 mm^2 and 1024 X 1024 pixel elements. A 2:1 fiber-optic taper is bonded directly to the active face of the CCD array, increasing the imaging area to approximately 50 X 50 mm^2 and increasing the pixel size to approximately 50 X 50 μm^2. The detector provides spatial sampling of ~35 μm in the center of the field of view due to the cone-beam configuration of the system. A Kodak MinR phosphor screen is mechanically pressed against the larger side of the fiber optic taper to provide x-ray sensitivity. Although the CCD–based detector does not measure individual x-ray energies it does provide substantially improved statistics due to its charge integration mode of operation. With the CCD-based detector a set of 1024 parallel projections is acquired in 2-3 seconds. For low-resolution screening studies (~180 projection sets) a data set is acquired in ~7 minutes; higher resolution data sets (~360 – 500 projection sets) are acquired in 15-25 minutes.

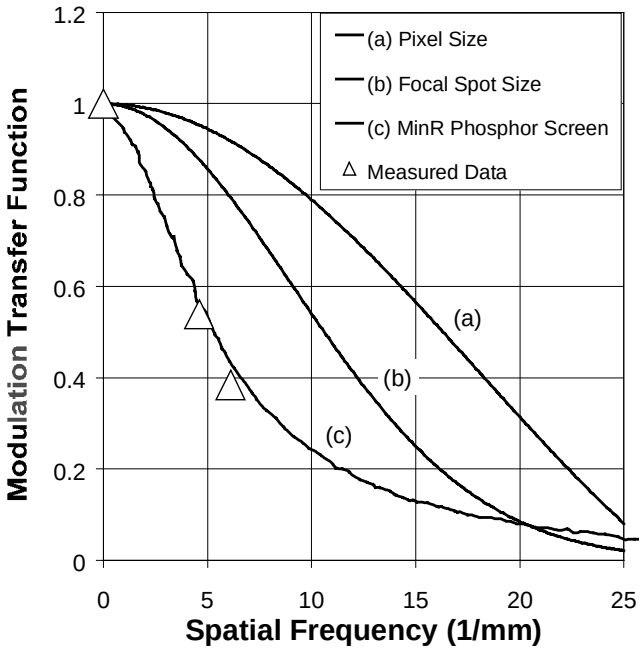

Figure 5. Calculated contributions to the CCD/Phosphor screen detector modulation transfer function due to (a) the detector pixel size, (b) the x-ray source size and (c) Kodak MinR phosphor screen blurring[24]. Three measured data points are also shown on the plot.

The system spatial resolution is limited by the pixel-sampling rate, the x-ray source size and blurring in the phosphor screen. Figure 5 shows the calculated contributions of these three components to the modulation transfer function (MTF) and three measured data points. Based on this figure, the detector phosphor screen blurring [24] is the resolution-limiting component and the MTF is reduced to approximately 20% for 40-μm layers of alternating high and low Z materials.

B. Software

Scanner motion and data acquisition are controlled through a graphical user interface on a Windows NT-based workstation. For image reconstruction the cone-beam data sets are treated as parallel stacks of fan-beam data. With the system's 10-degree cone-beam angle this approximation causes some loss of resolution near the edge of the z-axis field of view; we are working to implement a true 3-D reconstruction algorithm. The pseudo-parallel fan-beam projections are reconstructed using a fan-to-parallel-beam-rebinning algorithm followed by a filtered back-projection algorithm with a standard ramp filter. A maximum liklihood (ML) reconstruction algorithm has also been developed for the MicroCAT [20].

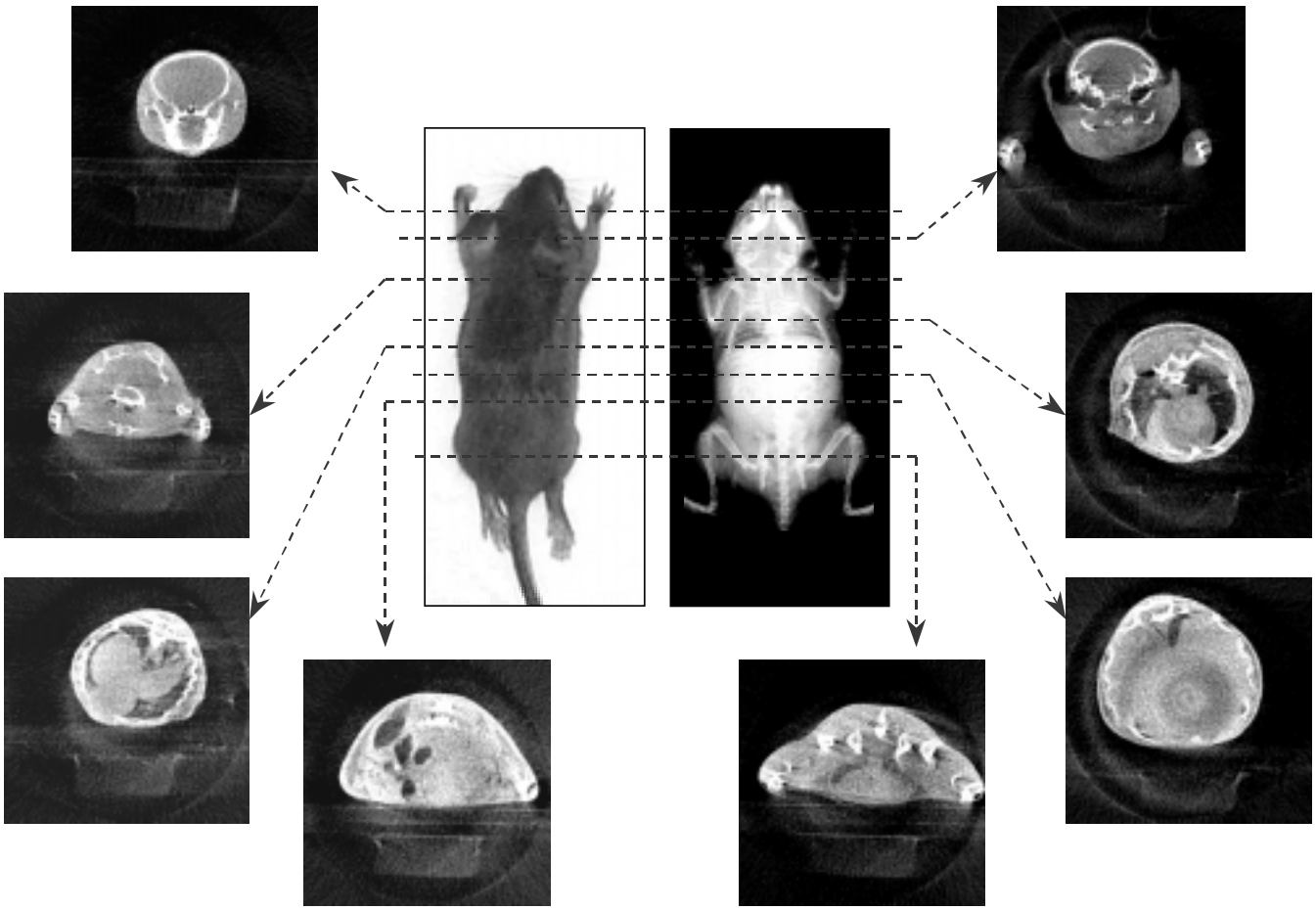

Figure 4. The first images obtained with the single-pixel CZT detector. Several 3-week old mice (~2.5 inches long excluding the tail) were studied. The x-ray tube was biased at 30 kV and the anode current was set to 0.3 mA for these acquisitions. The detector step was 250 μm. A filtered back-projection algorithm was used to reconstruct the images.

Work is underway to develop new image segmentation algorithms to automatically determine size and mass of various mouse organs in order to screen for abnormalities. These automated screening algorithms will be important in future large-population mouse mutagenesis studies.

III. EXPERIMENTAL RESULTS

A. CZT Detector

Images acquired with the single-pixel CZT detector are shown in Figure 4. Several 3-week old mice (~2.5 inches long excluding the tail) were studied. For these acquisitions the x-ray tube was biased at 30 kV and the anode current was set to 0.3 mA. A detector step size of 250 μm was employed, and a filtered back-projection algorithm with ramp filter was used to reconstruct the images.

As expected for a single-pixel system operating in pulse-mode, the image quality is limited by counting statistics. The textured noise visible in the images is similar to that often found in low-count nuclear medicine images reconstructed via filtered back-projection. A ML reconstruction algorithm designed to improve the image quality obtained with low-count data sets and to exploit the energy-dependent information contained in the data sets is reported elsewhere [20]. The pulse-mode image statistics are expected to improve significantly when the new multi-element detector becomes available. Circular artifacts visible in some of the images are due to inadequate detector calibration; an improved calibration algorithm is under development.

B. Phosphor screen/CCD Detector

Recent images obtained with the MicroCAT configured with the phosphor screen/CCD detector are shown in Figure 5. For these scans the x-ray tube was biased at 40 kV and the anode current was set to 0.4 mA. To improve the soft-tissue definition, an iodine contrast agent was IP injected into the mouse thirty minutes prior to data acquisition. While IV injection is typically the preferred route for contrast media, IP injection has been found to be much more convenient for mouse imaging, particularly in large population studies. The IP contrast agent opacifies the peritoneal fluid, providing high contrast separation between organs.

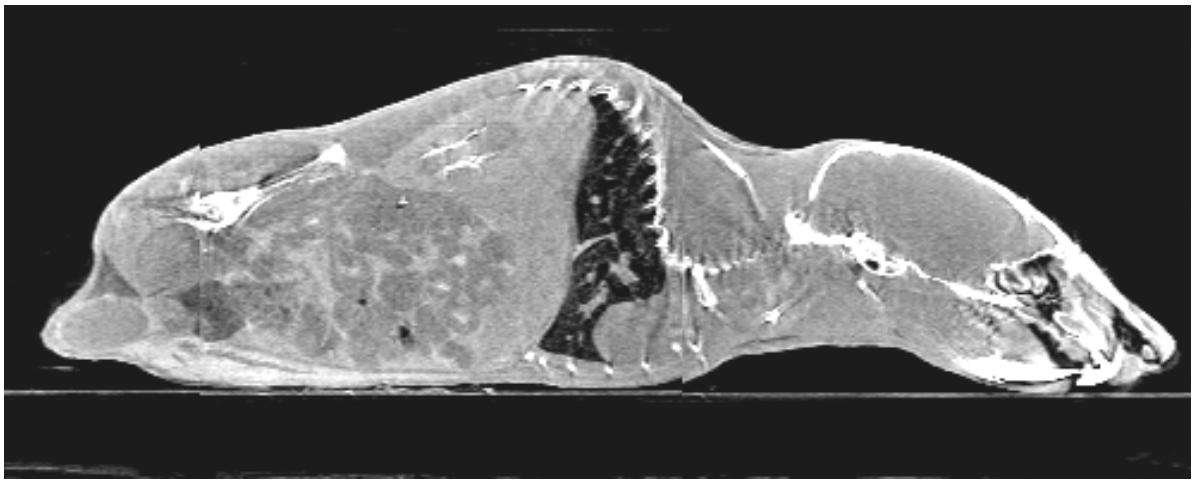

(a)

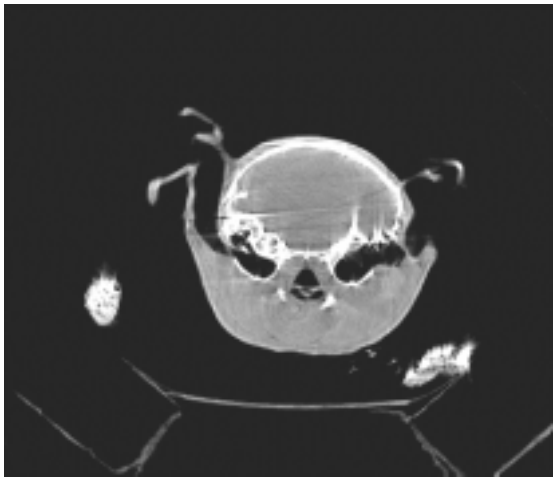

(b)

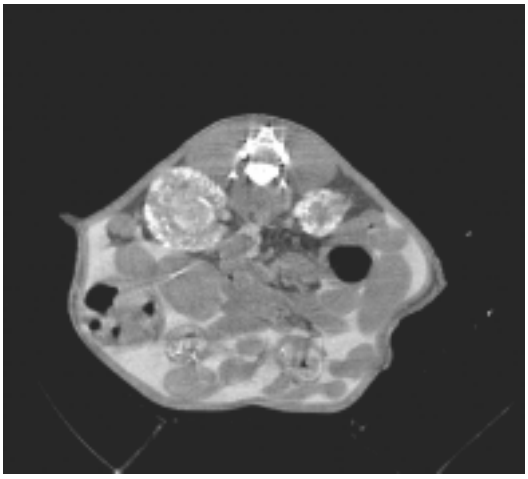

(c)

Figure 5. Recent images obtained with the phosphor screen/CCD detector. (a) Sagittal view of a 3-week old wild-type mouse with IP injected contrast media, (b) transverse skull scann of a 3-week old wild-type mouse, (c) transverse slice of an "orpk" polycystic kidney disorder mouse model showing the diseased kidneys[25].

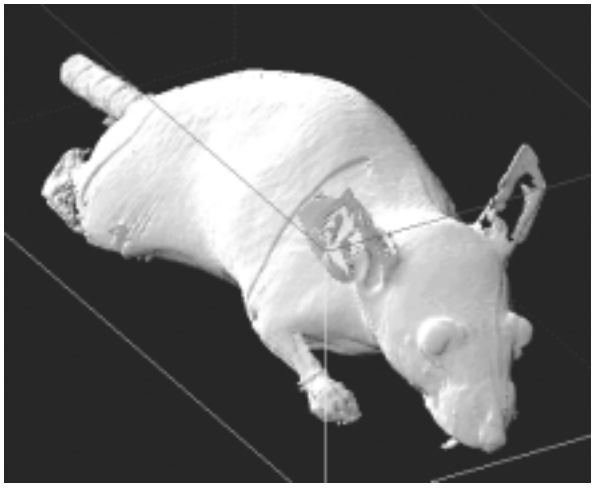

(a)

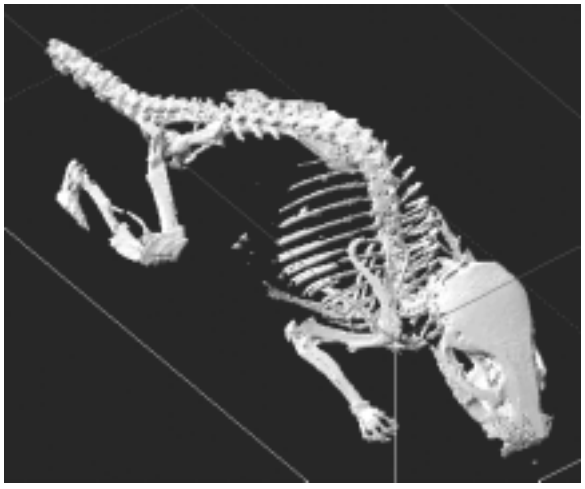

(b)

Figure 6. Surface rendering (a) and skeletal rendering (b) of a three-week old wild-type mouse obtained using the phosphor screen/CCD detector. The images were produced from the same data set.

Because the phosphor screen/CCD detector acquires multiple slices simultaneously, the system is well suited for volumetric data acquisition. Each scan acquires data for a 1.5 inch diameter x 1.5 inch long cylindrical volume. Whole body mouse data sets may be acquired in two or three scans. Figure 6 shows volume renderings of the mouse surface and skeleton. The skeletal image is obtained by placing a lower threshold on the reconstructed attenuation data.

Work is underway to eliminate artifacts appearing in images obtained with the phosphor screen/CCD detector. In particular, ring artifacts visible in homogeneous regions of the image are attributed to minor variations in the responses of pixels in the detector, and streak artifacts around bone/tissue interfaces are attributed to beam-hardening effects and aliasing. Potential corrections for the ring artifacts include improved detector calibration, a look-up table to correct for pixel-to-pixel response variations in the detector output and translation of the detector array during image acquisition to distribute each projection ray across several detector elements. Potential corrections for the streak artifacts include an improved beam-hardening correction algorithm and a modified filter function to suppress high frequency responses above the detector Nyquist frequency.

C. Image Comparison

The pulse-mode image quality is limited by the use of a single-pixel detector and the count-rate limitations imposed by the system dead time. It is anticipated the image statistics and acquisition times will improve when the pixilated detector becomes available, but the maximum x-ray pulse rate will still be significantly lower than that of the charge-integrating (phosphor screen/CCD) detector. Therefore, for general-purpose high-resolution CT studies the phosphor screen/CCD detector is believed to be the preferred tool due to the inherently superior statistics and shorter imaging time associated with this system. For studies requiring energy dependent attenuation data or for future ETCT studies the pulse-mode system shows promise.

SUMMARY

A new small animal imaging system has been developed. The system is designed for high spatial resolution and high throughput in order to screen large mouse populations in mutagenesis studies.

Two detectors were investigated. The first, a single-pixel CZT detector operating in pulse mode provides energy dependent data and is appropriate for dual modality CT/SPECT studies. A multi-element pixilated detector has been designed and will be incorporated into the scanner in the near future.

The second detector, a phosphor screen/CCD device, provides superior statistics and higher speed data acquisition. When operating in screening mode (180 projections) a volumetric data set may be acquired in approximately 7 minutes. IP injection has been found to be a convenient route for contrast media delivery to the mouse.

REFERENCES

[1] S.R. Cherry, *et al.* "MicroPet: a high resolution PET scanner for imaging small animals", *IEEE Trans. Nucl. Sci.*, vol 44, pp. 1161-1166 (1997).

[2] R. Lecomte, *et al*., "Initial results from the Sherbrooke avalanche photodiode positron tomograph", *IEEE Trans. Nucl. Sci*., vol. 43, pp. 1952-1957, (1996).

[3] D. A. Weber, *et al*., "Pinhole SPECT: A New Approach to In Vivo High Resolution SPECT Imaging in Small Laboratory Animals," *Journal of Nuclear Medicine*, vol. 35, pp. 342-348 (1994).

[4] L. Ploux, *et al*., "TOHR: Prototype Design and Characterization of an Original Small Animal Tomograph", Conference record of the 1997 Medical Imaging Conference, Paper M06-13, November 9-15, 1997.

[5] G.A. Johnson, *et al*., "MR microscopy in basic studies of brain structure and function," *Annals of the New York Academy of Sciences*, vol. 820, pp.139-148 (1997).

[6] M.S. Chawla, *et al.*, "In vivo MR vascular imaging using laser-polarized 3He microbubbles," *Proceedings of the National Academy of Sciences USA*, vol. 95, pp. 10832-10835 (1998).

[7] B.P. Flannery, *et al*., "Three-dimensional x-ray microtomography," *Science*, vol. 237, pp. 1439-1444 (1987).

[8] M.J. Flynn, *et al*., "Radiation dose for small field, high resolution computed tomography of bone," *Medical Physics*, vol. 24, p. 1048 (1997).

[9] D.W. Holdworth, *et al*., "A table-top CT system for high-resolution volume imaging," *SPIE*, vol. 1231, pp. 239-245 (1990).

[10] M.A. Kujoory, *et al*., "High resolution computed tomography of the normal rat nephrogram," *Investigative Radiology*, vol. 15, pp. 148-154 (1980).

[11] P. Burstein, *et al*., "The largest and smallest x-ray computed tomographic systems," *Nuclear Instruments and Methods in Physics*, vol. 221, pp. 207-212 (1984).

[12] F.H. Seguin, *et al*., "X-ray computed tomography with 50-μm resolution," *Applied Optics*, vol. 24, pp. 4117-4123 (1985).

[13] J.M. Boone, *et al*., "A fluoroscopy-based computed tomography system for small specimen research," *Investigative Radiology*, vol. 28, pp. 539-544 (1993).

[14] Oxford Model 5000, Oxford Technology Group, 275 Technology Circle, Scotts Valley, CA 95066.

[15] Detector Model eV 180, eV Products (a subsidiary of II-VI, Inc.), 375 Saxonburg Blvd., Saxonburg, PA 16056.

[16] O. Tousignant, *et al.*, "Transport properties and performance of CdZnTe strip detectors," *Conference Record of the 1997 IEEE Nuclear Science Symposium*, Paper N27-67, Albuquerque, November 1997.

[17] ORTEC Preamplifier Model 142A, EG&G ORTEC, 100 Midland Road, Oak Ridge, TN 7831-0895.

[18] ORTEC Amplifier Model 570, EG&G ORTEC, 100 Midland Road, Oak Ridge, TN 7831-0895.

[19] Oxford PCA3, Oxford Instruments Nuclear Measurements Group, 601 Oak Ridge Turnpike, Oak Ridge, TN, 37830-2560,

[20] S.S. Gleason, *et al*., "Reconstruction of High-Resolution, Multi-Energy, X-ray Computed Tomography Laboratory Mouse Images," paper M6-77, presented at the *1998 Medical Imaging Conference*, Toronto, November, 1998.

[21] R. E. Alvarez and A. Macovski, "Energy-selective reconstruction in X-ray computerized tomography," *Phys. Med. Biol*., vol. 21, pp. 733-744, 1976.

[22] J.A. Heanue, *et al*., "The Effects of Radionuclide Scatter in Emission-Transmission CT," *Conference record of the 1996 Medical Imaging Conference*, Paper M08-1, Anaheim, November 1996.

[23] Medoptics Corporation, 4588 S. Palo Verde Rd., Suite 405, Tuscon, AZ 85714.

[24] Kodak Technical Bulletin TI0997.

[25] Moyer, J.M, *et al.*, "Candidate gene associated with a mutation causing recessive polycystic kidney disease in mice," *Science*, 264:1329-1333, 1994.